with permeability κ. Based on the above assumptions, the governing equations can be expressed as follows [31].

Region I:

$$\begin{aligned}
\frac{\partial v_1}{\partial y} &= 0,\\
\rho_{\mathrm{f}}\frac{\partial u_1}{\partial t} &= -\frac{\partial P^*}{\partial x} + \mu_{\mathrm{f}}\left(1+\frac{1}{\beta}\right)\frac{\partial^2 u_1}{\partial y^2} + g(\rho_{\mathrm{f}}\beta_T)_{\mathrm{f}}(T_1 - T_{w2}),\\
(\rho c_p)_{\mathrm{f}}\frac{\partial T_1}{\partial t} &= k_{\mathrm{f}}\frac{\partial^2}{T_1}\partial y^2 + \mu_{\mathrm{f}}\left(1+\frac{1}{\beta}\right)\left(\frac{\partial u_1}{\partial y}\right)^2 + Q_1^*(T_1 - T_{w2}).
\end{aligned}$$

Region II:

$$\begin{aligned}
\frac{\partial v_2}{\partial y} &= 0,\\
\rho_{\mathrm{hnf}}\frac{\partial u_2}{\partial t} &= -\frac{\partial P^*}{\partial x} + \mu_{\mathrm{hnf}}\left(1+\frac{1}{\beta}\right)\frac{\partial^2 u_2}{\partial y^2} + \bigl((\rho\beta_T)_{\mathrm{hnf}}g\bigr)(T_2 - T_{w2})\\
&\quad - \frac{\mu_{\mathrm{hnf}}}{\kappa}\left(1+\frac{1}{\beta}\right)u_2,\\
(\rho c_p)_{\mathrm{hnf}}\frac{\partial T_2}{\partial t} &= k_{\mathrm{hnf}}\frac{\partial^2 T_2}{\partial y^2} + \mu_{\mathrm{hnf}}\left(1+\frac{1}{\beta}\right)\left(\frac{\partial u_2}{\partial y}\right)^2 + \frac{\mu_{\mathrm{hnf}}}{k}\left(1+\frac{1}{\beta}\right)u_2^2\\
&\quad + Q_2^*(T_2 - T_{w2}).
\end{aligned}$$

Region III:

$$\begin{aligned}
\frac{\partial v_3}{\partial y} &= 0,\\
\rho_{\mathrm{f}}\frac{\partial u_3}{\partial t} &= -\frac{\partial P^*}{\partial x} + \mu_{\mathrm{f}}\left(1+\frac{1}{\beta}\right)\frac{\partial^2 u_3}{\partial y^2} + g(\rho\beta_T)_{\mathrm{f}}(T_3 - T_{w2}),\\
(\rho c_p)_{\mathrm{f}}\frac{\partial T_3}{\partial t} &= k_{\mathrm{f}}\frac{\partial^2 T_3}{\partial y^2} + \mu_{\mathrm{f}}\left(1+\frac{1}{\beta}\right)\left(\frac{\partial u_3}{\partial y}\right)^2 + Q_3^*(T_1 - T_{w2}).
\end{aligned}$$

Boundary conditions:

$$\begin{aligned}
&u_1 = 0, \quad T_1 = T_{w2} \quad \text{at } y = -d,\\
&u_1 = u_2, \quad T_1 = T_2,\\
&\quad \mu_{\mathrm{f}}\left(1+\frac{1}{\beta}\right)\frac{\partial u_1}{\partial y} = \mu_{\mathrm{hnf}}\left(1+\frac{1}{\beta}\right)\frac{\partial u_2}{\partial y}, \quad k_{\mathrm{f}}\frac{\partial T_1}{\partial y} = k_{\mathrm{hnf}}\frac{\partial T_2}{\partial y} \quad \text{at } y = 0,\\
&u_2 = u_3, \quad T_2 = T_3,\\
&\quad \mu_{\mathrm{hnf}}\left(1+\frac{1}{\beta}\right)\frac{\partial u_2}{\partial y} = \mu_{\mathrm{f}}\left(1+\frac{1}{\beta}\right)\frac{\partial u_3}{\partial y}, \quad k_{\mathrm{hnf}}\frac{\partial T_2}{\partial y} = k_{\mathrm{f}}\frac{\partial T_3}{\partial y} \quad \text{at } y = d,\\
&u_3 = 0, \quad T_3 = T_{w1} \quad \text{at } y = 2d,
\end{aligned}$$

Table 1. Thermophysical properties of base fluid (blood) and nanoparticles (gold and titanium).

	Blood	Au	Ti
ρ (kg m^{-3})	1050	19282	4510
β_T (K^{-1})	$0.18 \cdot 10^{-5}$	$14 \cdot 10^{-6}$	$0.9 \cdot 10^{-5}$
k (W m^{-1}K^{-1})	0.52	310	20.9
c_p (J kg^{-1}K^{-1})	3617	129	540

where u_i, v_i, T_i, and Q_i^* ($i = 1, 2, 3$) are the velocities along x-direction, the velocities along y-direction, the temperatures, and the internal heat generation/absorption of regions I, II, and III, respectively. κ is the porous media, and β is the Casson parameter. The unsteady pressure gradient is given by

$$-\frac{1}{\rho_{\mathrm{f}}}\frac{\partial P^*}{\partial x} = A\big[1 + \varepsilon\exp(\mathrm{i}\omega t)\big],$$

where $\varepsilon \ll 1$ is a suitable chosen positive quantity, A is a known constant. Table 1 shows the thermophysical properties of blood and nanoparticles (gold and titanium) fluid. The physical characteristics of the nanofluid are defined as [32]:

$$\begin{aligned}
\frac{\mu_{\mathrm{hnf}}}{\mu_{\mathrm{f}}} &= \frac{1}{(1-\phi_{\mathrm{Ti}})^{2.5}(1-\phi_{\mathrm{Au}})^{2.5}},\\
\frac{\rho_{\mathrm{hnf}}}{\rho_{\mathrm{f}}} &= (1-\phi_{\mathrm{Au}})\left((1-\phi_{\mathrm{Ti}}) + \phi_{\mathrm{Ti}}\frac{\rho_{\mathrm{Ti}}}{\rho_{\mathrm{f}}}\right) + \phi_{\mathrm{Au}}\frac{\rho_{\mathrm{Au}}}{\rho_{\mathrm{f}}},\\
\frac{(\rho C_p)_{\mathrm{hnf}}}{(\rho C_p)_{\mathrm{f}}} &= (1-\phi_{\mathrm{Au}})\left((1-\phi_{\mathrm{Ti}}) + \phi_{\mathrm{Ti}}\frac{(\rho C_p)_{\mathrm{Ti}}}{(\rho C_p)_{\mathrm{f}}}\right) + \phi_{\mathrm{Au}}\frac{(\rho C_p)_{\mathrm{Au}}}{(\rho C_p)_{\mathrm{f}}},\\
\alpha_{\mathrm{hnf}} &= \frac{k_{\mathrm{hnf}}}{(\rho C_p)_{\mathrm{hnf}}},\\
\frac{(\rho\beta_t)_{\mathrm{hnf}}}{(\rho\beta_t)_{\mathrm{f}}} &= (1-\phi_{\mathrm{Au}})\left((1-\phi_{\mathrm{Ti}}) + \phi_{\mathrm{Ti}}\frac{(\rho\beta_t)_{\mathrm{Ti}}}{(\rho\beta_t)_{\mathrm{f}}}\right) + \phi_{\mathrm{Au}}\frac{(\rho\beta_t)_{\mathrm{Au}}}{(\rho\beta_t)_{\mathrm{f}}},\\
\frac{k_{\mathrm{hnf}}}{k_{\mathrm{bf}}} &= \frac{(k_{\mathrm{Au}} + (n-1)k_{\mathrm{bf}} - (n-1)\phi_{\mathrm{Au}}(k_{\mathrm{bf}} - k_{\mathrm{Au}}))k_{\mathrm{bf}}}{(k_{\mathrm{Au}} + (n-1)k_{\mathrm{bf}} + \phi_{\mathrm{Au}}(k_{\mathrm{bf}} - k_{\mathrm{Au}}))k_{\mathrm{f}}},
\end{aligned}$$

where

$$k_{\mathrm{bf}} = \frac{k_{\mathrm{f}}(k_{\mathrm{Ti}} + (n-1)k_{\mathrm{f}} - (n-1)\phi_{\mathrm{Ti}}(k_{\mathrm{f}} - k_{\mathrm{Ti}}))}{k_{\mathrm{Ti}} + (n-1)k_{\mathrm{f}} + \phi_{\mathrm{Ti}}(k_{\mathrm{f}} - k_{\mathrm{Ti}})}.$$

Similarity transformations:

$$\begin{gathered}
U_1 = \frac{\omega u_1}{A}, \qquad U_2 = \frac{\omega u_2}{A}, \qquad U_3 = \frac{\omega u_3}{A},\\
\theta_1 = \frac{T_1 - T_{w2}}{T_{w1} - T_{w2}}, \qquad \theta_2 = \frac{T_2 - T_{w2}}{T_{w1} - T_{w2}}, \qquad \theta_3 = \frac{T_3 - T_{w2}}{T_{w1} - T_{w2}},\\
P = \frac{P^*}{A\rho_f d}, \qquad \zeta = \frac{y}{d}, \qquad \eta = \frac{x}{d}, \qquad \tau = \omega t,
\end{gathered}$$

$$Gr = \frac{(\beta_T)_f g(T_{w1} - T_{w2})\omega d^2}{A\upsilon_f}, \qquad H^2 = \frac{\omega d^2}{\upsilon_f},$$
$$Q_1 = \frac{Q_1^* d^2}{\mu_f c_{p_f}}, \qquad Q_2 = \frac{Q_2^* d^2}{\mu_f c_{p_f}}, \qquad Q_3 = \frac{Q_3^* d^2}{\mu_f c_{p_f}}, \qquad Pr = \frac{\mu_f (c_p)_f}{k_f}.$$

Region I:

$$H^2 \frac{\partial U_1}{\partial \tau} = -H^2 \frac{\partial P}{\partial \eta} + \left(1 + \frac{1}{\beta}\right) \frac{\partial^2 U_1}{\partial \zeta^2} + Gr\,\theta_1, \tag{1}$$
$$H^2 \frac{\partial \theta_1}{\partial \tau} = \frac{1}{Pr} \frac{\partial^2 \theta_1}{\partial \zeta^2} + Ec\left(1 + \frac{1}{\beta}\right)\left(\frac{\partial U_1}{\partial \zeta}\right)^2 + Q_1 \theta_1. \tag{2}$$

Region II:

$$\frac{\rho_{\mathrm{hnf}}}{\rho_{\mathrm{f}}} H^2 \frac{\partial U_2}{\partial \tau} = -H^2 \frac{\partial P}{\partial \eta} + \frac{\mu_{\mathrm{hnf}}}{\mu_{\mathrm{f}}}\left(1 + \frac{1}{\beta}\right) \frac{\partial^2 U_2}{\partial \zeta^2} + \frac{(\rho\beta_T)_{\mathrm{hnf}}}{(\rho\beta_T)_{\mathrm{f}}} Gr\,\theta_2, \tag{3}$$
$$-\frac{\mu_{\mathrm{hnf}}}{\mu_{\mathrm{f}}}\left(1 + \frac{1}{\beta}\right)\sigma^2 U_2 \frac{(\rho c_p)_{\mathrm{hnf}}}{(\rho c_p)_{\mathrm{f}}} H^2 \frac{\partial \theta_2}{\partial \tau}$$
$$= \frac{k_{\mathrm{hnf}}}{k_{\mathrm{f}}} \frac{1}{Pr} \frac{\partial^2 \theta_2}{\partial \zeta^2} + \frac{\mu_{\mathrm{hnf}}}{\mu_{\mathrm{f}}}\left(1 + \frac{1}{\beta}\right) Ec \left(\frac{\partial u_2}{\partial \zeta}\right)^2 + \frac{\mu_{\mathrm{hnf}}}{\mu_{\mathrm{f}}}\left(1 + \frac{1}{\beta}\right) Ec\,\sigma^2 U_2^2$$
$$+ Q_2 \theta_2. \tag{4}$$

Region III:

$$H^2 \frac{\partial U_3}{\partial \tau} = -H^2 \frac{\partial P}{\partial \eta} + \left(1 + \frac{1}{\beta}\right) \frac{\partial^2 U_3}{\partial \zeta^2} + Gr\,\theta_3, \tag{5}$$
$$H^2 \frac{\partial \theta_3}{\partial t} = \frac{1}{Pr} \frac{\partial^2 \theta_3}{\partial \zeta^2} + Ec\left(1 + \frac{1}{\beta}\right)\left(\frac{\partial U_3}{\partial \zeta}\right)^2 + Q_3 \theta_3. \tag{6}$$

The nondimensional form of the boundary conditions are:

$$\begin{aligned}
&U_1 = 0, \quad \theta_1 = 0 \quad \text{at } \zeta = -1, \\
&U_1 = U_2, \quad \theta_1 = \theta_2, \quad \frac{\partial U_1}{\partial \zeta} = \frac{\mu_{\mathrm{hnf}}}{\mu_{\mathrm{f}}} \frac{\partial U_2}{\partial \zeta}, \quad \frac{\partial \theta_1}{\partial \zeta} = \frac{k_{\mathrm{hnf}}}{k_{\mathrm{f}}} \frac{\partial \theta_2}{\partial \zeta} \quad \text{at } \zeta = 0, \\
&U_2 = U_3, \quad \theta_2 = \theta_3, \quad \frac{\mu_{\mathrm{hnf}}}{\mu_{\mathrm{f}}} \frac{\partial U_2}{\partial \zeta} = \frac{\partial U_3}{\partial \zeta}, \quad \frac{k_{\mathrm{hnf}}}{k_{\mathrm{f}}} \frac{\partial \theta_2}{\partial \zeta} = \frac{\partial \theta_3}{\partial \zeta} \quad \text{at } \zeta = 1, \\
&U_3 = 0, \quad \theta_3 = 1 \quad \text{at } \zeta = 2.
\end{aligned} \tag{7}$$

3 Solution of the problem

The solution equations for U_i and θ_i $(i = 1, 2, 3)$ can be written as follows [25]:

$$U_i(\zeta, t) = U_{i,1}(\zeta) + \varepsilon \mathrm{e}^{\mathrm{i}\omega t} U_{i,2}(\zeta), \qquad \theta_i(\zeta, t) = \theta_{i,1}(\zeta) + \varepsilon \mathrm{e}^{\mathrm{i}\omega t} \theta_{i,2}(\zeta). \tag{8}$$

By substituting Eq. (8) into Eqs. (1)–(7) and setting the coefficients of similar powers of ε to zero, we derive the zeroth- and first-order equations along with their corresponding boundary and interface conditions as follows:

$$\left(1+\frac{1}{\beta}\right)\left(\frac{\mathrm{d}^2}{\mathrm{d}\zeta^2}U_{11}(\zeta)\right)+H^2+Gr\,\theta_{11}(\zeta)=0, \tag{9}$$

$$\left(1+\frac{1}{\beta}\right)\left(\frac{\mathrm{d}^2}{\mathrm{d}\zeta^2}U_{12}(\zeta)\right)-\mathrm{i}H^2U_{12}(\zeta)+H^2+Gr\,\theta_{12}(\zeta)=0, \tag{10}$$

$$\frac{\frac{\mathrm{d}^2}{\mathrm{d}\zeta^2}\theta_{11}(\zeta)}{Pr}+Q_1\theta_{11}(\zeta)+Ec\left(1+\frac{1}{\beta}\right)\left(\frac{\mathrm{d}}{\mathrm{d}\zeta}U_{11}(\zeta)\right)^2=0, \tag{11}$$

$$\begin{aligned}&\frac{\frac{\mathrm{d}^2}{\mathrm{d}\zeta^2}\theta_{12}(\zeta)}{Pr}-\mathrm{i}H^2\theta_{12}(\zeta)+Q_1\theta_{12}(\zeta)\\&\quad+2Ec\left(1+\frac{1}{\beta}\right)\left(\frac{\mathrm{d}}{\mathrm{d}\zeta}U_{11}(\zeta)\right)\left(\frac{\mathrm{d}}{\mathrm{d}\zeta}U_{12}(\zeta)\right)=0,\end{aligned} \tag{12}$$

$$\begin{aligned}&\frac{\mu_{\mathrm{hnf}}}{\mu_f}\left(1+\frac{1}{\beta}\right)\left(\frac{\mathrm{d}^2}{\mathrm{d}\zeta^2}U_{21}(\zeta)\right)-\frac{\mu_{\mathrm{hnf}}}{\mu_f}\left(1+\frac{1}{\beta}\right)\sigma^2U_{21}(\zeta)\\&\quad+H^2+\frac{(\rho\beta_T)_{\mathrm{hnf}}}{(\rho\beta_T)_f}Gr\,\theta_{21}(\zeta)=0,\end{aligned} \tag{13}$$

$$\begin{aligned}&\frac{\mu_{\mathrm{hnf}}}{\mu_f}\left(1+\frac{1}{\beta}\right)\left(\frac{\mathrm{d}^2}{\mathrm{d}\zeta^2}U_{22}(\zeta)\right)-\mathrm{i}\frac{\rho_{\mathrm{hnf}}}{\rho_f}H^2U_{22}(\zeta)\\&\quad-\frac{\mu_{\mathrm{hnf}}}{\mu_f}\left(1+\frac{1}{\beta}\right)\sigma^2U_{22}(\zeta)+H^2+\frac{(\rho\beta_T)_{\mathrm{hnf}}}{(\rho\beta_T)_f}Gr\,\theta_{22}(\zeta)=0,\end{aligned} \tag{14}$$

$$\begin{aligned}&\frac{k_{\mathrm{hnf}}}{k_f}\frac{1}{Pr}\left(\frac{\mathrm{d}^2}{\mathrm{d}\zeta^2}\theta_{21}(\zeta)\right)+\frac{\mu_{\mathrm{hnf}}}{\mu_f}Ec\left(1+\frac{1}{\beta}\right)\left(\frac{\mathrm{d}}{\mathrm{d}\zeta}U_{21}(\zeta)\right)^2\\&\quad+\frac{\mu_{\mathrm{hnf}}}{\mu_f}Ec\left(1+\frac{1}{\beta}\right)\sigma^2U_{21}^2(\zeta)+Q_2\theta_{21}(\zeta)=0,\end{aligned} \tag{15}$$

$$\begin{aligned}&\frac{k_{\mathrm{hnf}}}{k_f}\frac{1}{Pr}\left(\frac{\mathrm{d}^2}{\mathrm{d}\zeta^2}\theta_{22}(\zeta)\right)+2\frac{\mu_{\mathrm{hnf}}}{\mu_f}Ec\left(1+\frac{1}{\beta}\right)\left(\frac{\mathrm{d}}{\mathrm{d}\zeta}U_{21}(\zeta)\right)\left(\frac{\mathrm{d}}{\mathrm{d}\zeta}U_{22}(\zeta)\right)\\&\quad-\mathrm{i}\frac{(\rho c_p)_{\mathrm{hnf}}}{(\rho c_p)_f}H^2\theta_{22}(\zeta)+Q_2\theta_{22}(\zeta)\\&\quad+2\frac{\mu_{\mathrm{hnf}}}{\mu_f}Ec\left(1+\frac{1}{\beta}\right)\sigma^2U_{21}(\zeta)U_{22}(\zeta)=0,\end{aligned} \tag{16}$$

$$\left(1+\frac{1}{\beta}\right)\left(\frac{\mathrm{d}^2}{\mathrm{d}\zeta^2}U_{31}(\zeta)\right)+H^2+Gr\,\theta_{31}(\zeta)=0, \tag{17}$$

$$\left(1+\frac{1}{\beta}\right)\left(\frac{\mathrm{d}^2}{\mathrm{d}\zeta^2}U_{32}(\zeta)\right)-\mathrm{i}H^2U_{32}(\zeta)+H^2+Gr\,\theta_{32}(\zeta)=0, \tag{18}$$

$$\frac{1}{Pr}\frac{\mathrm{d}^2}{\mathrm{d}\zeta^2}\theta_{31}(\zeta) + Q_3\theta_{31}(\zeta) + Ec\left(1+\frac{1}{\beta}\right)\left(\frac{\mathrm{d}}{\mathrm{d}\zeta}U_{31}(\zeta)\right)^2 = 0, \tag{19}$$

$$\begin{aligned}&\frac{1}{Pr}\frac{\mathrm{d}^2}{\mathrm{d}\zeta^2}\theta_{32}(\zeta) - \mathrm{i}H^2\theta_{32}(\zeta) + Q_3\theta_{32}(\zeta)\\ &\quad + 2Ec\left(1+\frac{1}{\beta}\right)\left(\frac{\mathrm{d}}{\mathrm{d}\zeta}U_{31}(\zeta)\right)\left(\frac{\mathrm{d}}{\mathrm{d}\zeta}U_{32}(\zeta)\right) = 0\end{aligned} \tag{20}$$

with boundary conditions

$$U_{11} = 0, \quad \theta_{11} = 0, \quad U_{12} = 0, \quad \theta_{12} = 0 \quad \text{at} \quad \zeta = -1,$$

$$\begin{aligned}&U_{11} = U_{21}, \quad \theta_{11} = \theta_{21},\\ &\quad \frac{\partial U_{11}}{\partial \zeta} = \frac{\mu_{\mathrm{hnf}}}{\mu_{\mathrm{f}}}\frac{\partial U_{21}}{\partial \zeta}, \quad \frac{\partial \theta_{11}}{\partial \zeta} = \frac{k_{\mathrm{hnf}}}{k_{\mathrm{f}}}\frac{\partial \theta_{21}}{\partial \zeta} \quad \text{at } \zeta = 0,\\ &U_{12} = U_{22}, \quad \theta_{12} = \theta_{22},\\ &\quad \frac{\partial U_{12}}{\partial \zeta} = \frac{\mu_{\mathrm{hnf}}}{\mu_{\mathrm{f}}}\frac{\partial U_{22}}{\partial \zeta}, \quad \frac{\partial \theta_{12}}{\partial \zeta} = \frac{k_{\mathrm{hnf}}}{k_{\mathrm{f}}}\frac{\partial \theta_{22}}{\partial \zeta} \quad \text{at } \zeta = 0,\end{aligned}$$

$$\begin{aligned}&U_{21} = U_{31}, \quad \theta_{21} = \theta_{31},\\ &\quad \frac{\mu_{\mathrm{hnf}}}{\mu_{\mathrm{f}}}\frac{\partial U_{21}}{\partial \zeta} = \frac{\partial U_{31}}{\partial \zeta}, \quad \frac{k_{\mathrm{hnf}}}{k_{\mathrm{f}}}\frac{\partial \theta_{21}}{\partial \zeta} = \frac{\partial \theta_{31}}{\partial \zeta} \quad \text{at } \zeta = 1,\\ &U_{22} = U_{32}, \quad \theta_{22} = \theta_{32},\\ &\quad \frac{\mu_{\mathrm{hnf}}}{\mu_{\mathrm{f}}}\frac{\partial U_{22}}{\partial \zeta} = \frac{\partial U_{32}}{\partial \zeta}, \quad \frac{k_{\mathrm{hnf}}}{k_{\mathrm{f}}}\frac{\partial \theta_{22}}{\partial \zeta} = \frac{\partial \theta_{32}}{\partial \zeta} \quad \text{at } \zeta = 1,\end{aligned}$$

$$U_{31} = 0, \quad \theta_{31} = 1, \quad U_{32} = 0, \quad \theta_{32} = 1 \quad \text{at } \zeta = 2.$$

Since the solutions of Eqs. (9)–(20) along with their boundary interface conditions can be found easily by integrating the equations (see Umavathi and Hemavathi [31]).

The dimensionless Nusselt number is given by

$$Nu = -(\theta_i')_{\zeta=-1,2} = -\big(\theta_{i,1}' + \varepsilon\theta_{i,2}'\mathrm{e}^{\mathrm{i}t}\big)_{\zeta=-1,2}, \quad \text{where } i = 1, 3.$$

4 Results and discussion

The purpose of this section is to depict the convective transport of pulsatile multilayer flow of titanium (Ti) and gold (Au) based blood hybrid nanofluid in a composite porous channel with thermal radiation and heat source/sink parameters in three different regions effects. It is assumed that the momentum and thermal aspects of hybrid across the contact are all uninterrupted. Using the perturbation approach, analytical calculations have been done to analyze the multifluid model for several relevant parameters, including the Casson parameter β, Grashof number Gr, frequency parameter H, porous parameter σ, Eckert

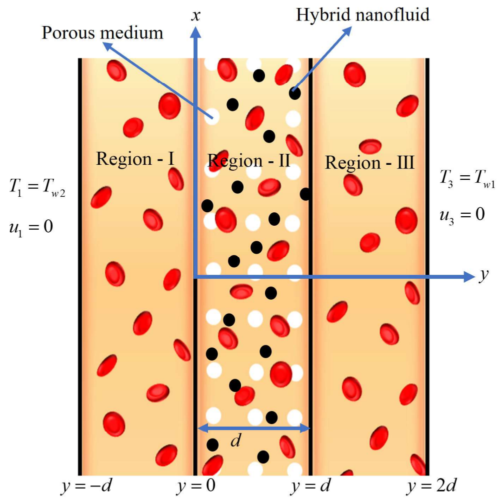

Figure 1. Geometry of the problem.

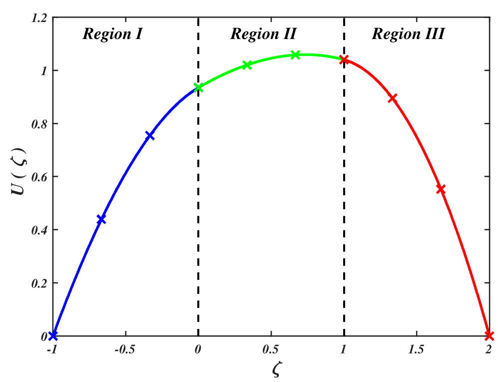

Figure 2. Comparison of present results with Umavati and Hemavati [31].

number Ec, nanoparticle volume fraction $\phi = \phi_{\mathrm{Au}} + \phi_{\mathrm{Ti}} = 0.05$, heat source/sink parameters Q_1, Q_2, and Q_3, time t on Ti–Au/ blood hybrid nanofluid velocities $U_s(\zeta)$ and $U_t(\zeta)$ and temperature $\theta_s(\zeta)$ and $\theta_t(\zeta)$ are visualized and elaborately discussed. Figure 1 shows the three different heat source/sink parameter regions. The first region between -1 and 0 is blue, the second region between 0 and 1 is green, and the third region between 1 and 2 is red, respectively. Figure 2 shows the comparison of present results with Umavati and Hemavati [31]. The results show good agreement with the Umavati and Hemavati [31].

Figures 3(a)–3(d) manifested the steady velocity profiles $U_s(\zeta)$ for Casson parameter ($\beta = 0.7, 0.8, 0.9$), Grashof number ($Gr = 0.2, 0.3, 0.4$), frequency parameter ($H = 2.0, 2.2, 2.4$), porous parameter ($\sigma = 2.2, 2.4, 2.6$) through three different regions. Figure 3(a) demonstrates that improving Casson parameter β tend to increase the $U_s(\zeta)$.

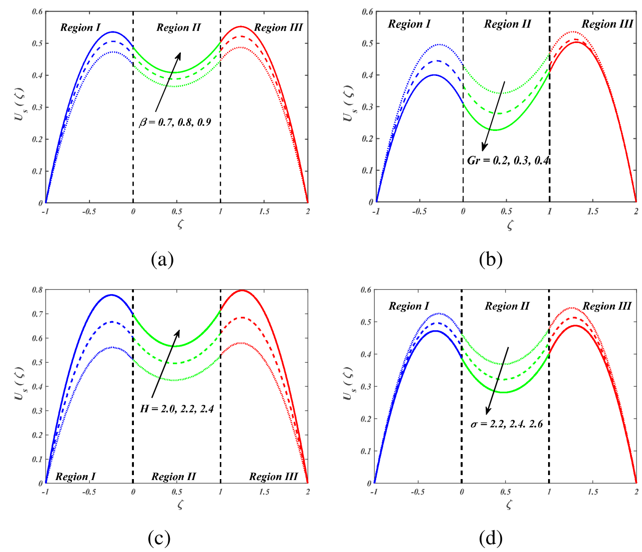

Figure 3. Steady velocity profiles for different values of (a) Casson parameter β, (b) Grashof number Gr, (c) frequency parameter H, and (d) porous parameter σ.

This is due to the fact that an increase in β creates a rise in fluid viscosity, and it follows that a greater viscosity produces a larger velocity. The extent of the growth, however, differs depending on the region. The amplitude of the velocity increase is less in region II when compared to the region I and in region II when compared to region III because the fluid is saturated with porous medium in the middle of the channel. The Casson parameter within the velocity profile can be relevant for understanding blood flow dynamics, particularly during cardiac cycles. By adjusting this parameter, researchers can model the impact of non-Newtonian behavior on blood flow in arteries and predict changes in shear stress, which is vital for assessing the risk of cardiovascular diseases. Figure 3(b) displays how the $U_s(\zeta)$ profile and Gr is inversely connected. This graph demonstrates that the velocity profiles decrease with increasing amounts of Grashof number. However, the rate of expansion varies depending on the area. Because the fluid is saturated with porous medium in the center of the channel, the amplitude of the velocity increase is smaller in region II than in region I and in region II than in region III. In Fig. 3(c) the behavior of the H on velocity $U_s(\zeta)$ is portrayed. This graph demonstrates that the higher values of H increase all three regions of the $U_s(\zeta)$. Physically, this corresponds to the ratio of pulsatile flow oscillation frequency to body acceleration frequency. However, compared to the centre of the channel, the effect of augmentation on the velocity field is more pronounced towards the right and left walls of the channel. Figure 3(d) illustrates how the porous parameter σ influences on velocity profile $U_s(\zeta)$. According to this graph, $U_s(\zeta)$ is diminished by expanding values in the σ. Physically, the porous media causes the fluid motion to produce second-order quadratic drag, which lowers the velocity in the boundary layer. Comparing region I and region III to the mid-channel (nanofluid saturated with porous media), the impact of suppression is dominant (clear viscous). When the

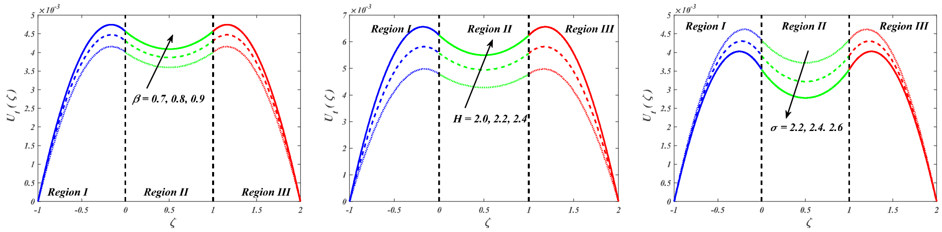

(a) (b) (c)

Figure 4. Unsteady velocity profiles for different values of (a) Casson parameter β, (b) frequency parameter H, and (c) porous parameter σ.

tube is completely filled with one fluid, this is another typical outcome that is seen. This parameter adjustment helps in modeling the behavior of fluids in tissues or porous structures during dynamic processes, such as pulsatile blood flow in arteries. Lowering the porous parameter can represent changes in tissue elasticity or permeability, aiding in the understanding of diseases like hypertension, arteriosclerosis, and tumor growth within porous tissues.

The consequence of the Casson parameter ($\beta = 0.7, 0.8, 0.9$), frequency parameter ($H = 2.0, 2.2, 2.4$), and porous parameter ($\sigma = 2.2, 2.4, 2.6$) over three different regions on unsteady velocity $U_t(\zeta)$ is represented in Figs. 4(a)–4(c). Figure 4(a) illustrates how the Casson parameter β influence on velocity profile $U_t(\zeta)$. According to this graph, $U_t(\zeta)$ is augmented by expanding values in β. Physically, an increase in β creates a rise in fluid viscosity, and it follows that a greater viscosity produces a larger velocity. Comparing region I and region III to the mid-channel (nanofluid saturated with porous media), the impact of suppression is dominant (clear viscous). When the tube is completely filled with one fluid, this is another typical outcome that is seen. Figure 4(b) demonstrates that improving frequency parameter H tends to increase the $U_t(\zeta)$. Physically, this corresponds to the ratio of pulsatile flow oscillation frequency to body acceleration frequency. The extent of the growth, however, differs depending on the region. The amplitude of the velocity increase is less in region II when compared to the region I and in region II when compared to region III because the fluid is saturated with porous medium in the middle of the channel. This modification may indicate disorders such as bradycardia or other heart rhythm irregularities, delivering information about the influence on hemodynamics as well as possible health concerns. Understanding these slower frequency patterns is critical in diagnosing, controlling, and forecasting the consequences of cardiac diseases on blood flow and tissue perfusion. In Fig. 4(c) the behavior of σ on velocity $U_t(\zeta)$ is portrayed. This graph demonstrates that the higher values of σ diminish all three regions of $U_t(\zeta)$. Physically, the porous media causes the fluid motion to produce second-order quadratic drag, which lowers the velocity in the boundary layer. However, compared to the centre of the channel, the effect of augmentation on the velocity field is more pronounced towards the right and left walls of the channel.

Figures 5(a)–5(f) manifesting the steady temperature profiles $\theta_s(\zeta)$ has been examined for Casson parameter ($\beta = 0.7, 0.8, 0.9$), frequency parameter ($H = 2.0, 2.2, 2.4$),

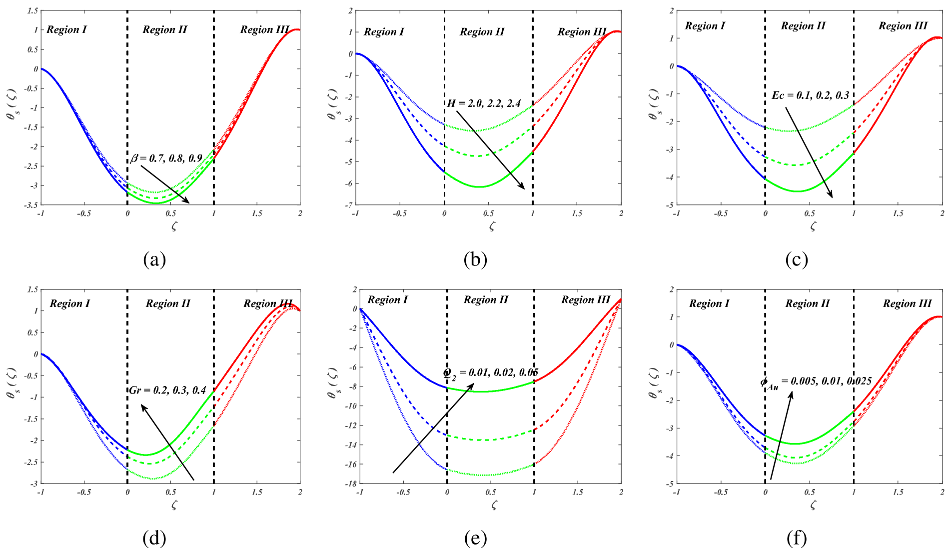

Figure 5. Steady temperature profiles for different values of (a) Casson parameter β, (b) frequency parameter H, (c)Eckert number Ec, (d) Grashof number Gr, (e) heat source/sink parameters Q_2, and (f) nanoparticle volume fraction ϕ_{Au}.

Eckert number ($Ec = 0.1,\ 0.2,\ 0.3$), Grashof number ($Gr = 0.2,\ 0.3,\ 0.4$), heat source/sink parameters ($Q_2 = 0.01,\ 0.02,\ 0.05$), and nanoparticle volume fraction ($\phi = 0.005$, 0.010, 0.025) through three different regions. Figure 5(a) demonstrates that improving Casson parameter β tends to diminution of $\theta_s(\zeta)$. This is due to the fact that an decrease in β creates a rise in fluid temperature, and it follows that a lesser viscosity produces a larger temperature. The extent of the growth, however, differs depending on the region. The amplitude of the temperature increase is less in region II when compared to the region I and in region II when compared to region III because the fluid is saturated with porous medium in the middle of the channel. In Fig. 5(b) the behavior of the H on temperature profiles $\theta_s(\zeta)$ is portrayed. This graph demonstrates that the higher values of H reduce all three regions of the $\theta_s(\zeta)$. Physically, this corresponds to the ratio pulsatile flow oscillation frequency to body acceleration frequency. However, compared to the centre of the channel, the effect of diminution on the temperature is more pronounced towards the right and left walls of the channel. In Fig. 5(c) the behavior of Ec on temperature profiles $\theta_s(\zeta)$ is portrayed. This graph demonstrates that the higher values of Ec reduce all three regions of $\theta_s(\zeta)$. Physically, the higher Ec produces more kinetic energy, causing particles to collide more frequently and dissipate energy. As a result, kinetic energy is converted into thermal energy. However, compared to the centre of the channel, the effect of diminution on the temperature is more pronounced towards the right and left walls of the channel. Figure 5(d) displays how $\theta_s(\zeta)$ profile and Gr are inversely connected. This graph demonstrates the temperature profile intensifications with increasing amounts of Grashof number. However, the rate of expansion varies depending on the area. Because the fluid is saturated with porous medium in the center of the channel, the amplitude of

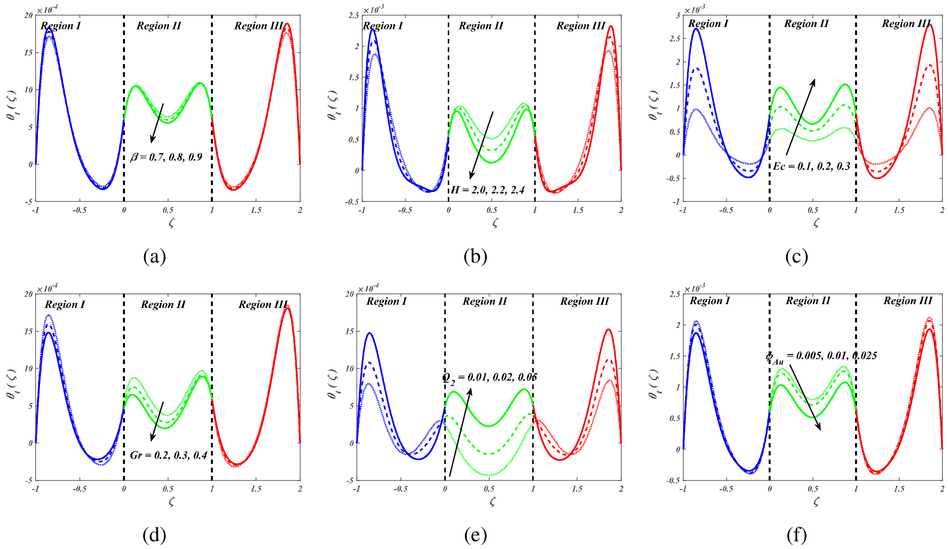

Figure 6. Unsteady temperature profiles for different values of (a) Casson parameter β, (b) frequency parameter H, (c) Eckert number Ec, (d) Grashof number Gr, (e) heat source/sink parameters Q_2, and (f) nanoparticle volume fraction ϕ_{Au}.

the temperature increase is smaller in region II than in region I and in region II than in region III. In Fig. 5(e) the behavior of Q_2 on temperature $\theta_s(\zeta)$ is portrayed. This graph demonstrates that the higher values of Q_2 increase all three regions of the $\theta_s(\zeta)$. However, compared to the centre of the channel, the effect of augmentation on the velocity field is more pronounced towards the right and left walls of the channel. It depicts situations when the amount of heat input or removal changes over time, such as when a person's body temperature is controlled by a fever or while receiving thermal therapy for medical conditions. Understanding how this parameter fluctuation affects different medical applications, such as hyperthermia therapies and thermal ablation techniques for tumor therapy, aids in the optimization of thermal management tactics. In Fig. 5(f) the behavior of ϕ_{Au} on temperature profiles $\theta_s(\zeta)$ is portrayed. This graph demonstrates that the higher values of ϕ_{Au} rises all three regions of $\theta_s(\zeta)$. One may explain this outcome by claiming that when nanoparticles are introduced to pure fluid, the fluid's density rises, and the fluid becomes denser, which causes the fluid's momentum to increase in the channel. However, compared to the centre of the channel, the effect of diminution on the temperature is more pronounced towards the right and left walls of the channel.

Figures 6(a)–6(f) manifesting the unsteady temperature profiles $\theta_t(\zeta)$ has been examined for Casson parameter ($\beta = 0.7,\ 0.8,\ 0.9$), frequency parameter ($H = 2.0,\ 2.2,\ 2.4$), Eckert number ($Ec = 0.1,\ 0.2,\ 0.3$), Grashof number ($Gr = 0.2,\ 0.3,\ 0.4$), heat source/sink parameters ($Q_2 = 0.01,\ 0.02,\ 0.05$), and nanoparticle volume fraction ($\phi = 0.005,\ 0.010,\ 0.025$) through three different regions. Figure 6(a) demonstrates that improving Casson parameter β tends to diminution of $\theta_t(\zeta)$. This is due to the fact that an decrease in β creates a rise in fluid temperature, and it follows that a lesser viscosity produces

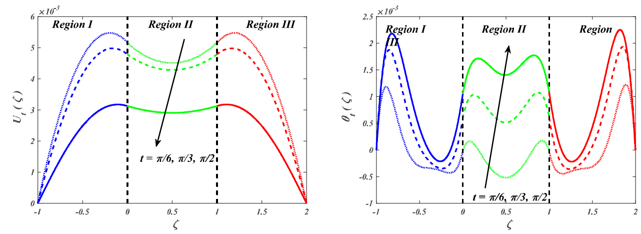

(a) (b)

Figure 7. Effect of time t on (a) unsteady velocity profile and (b) unsteady temperature profile.

Table 2. Values of Nu for different values of β, Gr, and σ with $\phi_{\mathrm{Au}} = \phi_{\mathrm{Ti}} = 0$, $Ec = Q_1 = Q_2 = Q_3 = 0.1$, $t = \pi/3$, and $H = 1$.

β	Gr	σ	Nu	
			$\zeta = -1$	$\zeta = 2$
0.5	0	0	1.46183	−0.46422
1.0	0	0	1.41708	−0.41947
inf	0	0	1.28284	−0.28523
0.5	0.1	0	1.47938	−0.43674
1.0	0.1	0	1.44314	−0.37846
inf	0.1	0	1.33382	−0.20460
0.5	0	2	1.72231	−0.72470
1.0	0	2	1.80780	−0.81019
inf	0	2	2.06429	−1.06668

nanoparticles. Understanding how this parameter affects heat transfer is crucial for optimizing applications like targeted hyperthermia treatments and controlled drug release within biological systems, ensuring the safety and effectiveness of these therapies.

Figures 7(a) and 7(b) manifesting the unsteady velocity $U_t(\zeta)$ and unsteady temperature profiles $\theta_t(\zeta)$ has been examined for time series parameter ($t = \pi/6$, $\pi/3$, $\pi/2$) through three different regions. In Fig. 7(a) the behavior of Q_2 on temperature $U_t(\zeta)$ is portrayed. This graph demonstrates that the higher values of t diminish all three regions of $U_t(\zeta)$. However, the rate of expansion varies depending on the area. Because the fluid is saturated with porous medium in the center of the channel, the amplitude of the temperature increase is smaller in region II than in region I and in region II than in region III. Figure 7(b) displays how $\theta_t(\zeta)$ profile and t are inversely connected. This graph demonstrates the temperature profile developments with increasing amounts of t. The amplitude of the temperature increase is less in region II when compared to the region I and in region II when compared to region III because the fluid is saturated with porous medium in the middle of the channel.

At $\zeta = -1$ and $\zeta = 2$, the outcomes of Nu for diverse aspects of β, Gr, and σ with Au–Ti hybrid nanofluids are taken as absent (see Table 2). From this we observed that Nu increases in $\zeta = -1$ with various values of β, Gr, and σ. In Table 3, at $\zeta = -1$ and $\zeta = 2$, the outcomes of Nu for diverse aspects of β, H, Gr, Ec, Q_1, Q_2, Q_3, and σ with Au–Ti hybrid nanofluids are taken as 0.025 and $t = \pi/3$. From this we observed that Nu diminishes the larger values of Ec, Q_1, Q_2, and Q_3.

Table 3. Values of Nu for different values of H, Gr, σ, Ec, Q_1, Q_2, and Q_3 with $\phi_{\mathrm{Au}} = \phi_{\mathrm{Ti}} = 0.025$ and $t = \pi/3$.

β	H	Gr	σ	Ec	Q_1	Q_2	Q_3	Nu	
								$\zeta = -1$	$\zeta = 2$
0.5	2.0	0.1	2.0	0.20	0.10	0.20	0.10	0.79656	0.42256
1.0	2.0	0.1	2.0	0.20	0.10	0.20	0.10	0.55100	0.82082
1.5	2.0	0.1	2.0	0.20	0.10	0.20	0.10	0.37220	1.09330
1.0	0.5	0.1	2.0	0.20	0.10	0.20	0.10	0.90581	0.03709
1.0	1.0	0.1	2.0	0.20	0.10	0.20	0.10	0.94120	0.08734
1.0	1.5	0.1	2.0	0.20	0.10	0.20	0.10	0.91409	0.25627
1.0	2.0	0.2	2.0	0.20	0.10	0.20	0.10	0.38569	1.46968
1.0	2.0	0.3	2.0	0.20	0.10	0.20	0.10	0.47236	1.92933
1.0	2.0	0.4	2.0	0.20	0.10	0.20	0.10	0.71853	2.44020
1.0	2.0	0.1	2.5	0.20	0.10	0.20	0.10	0.83971	0.49118
1.0	2.0	0.1	3.0	0.20	0.10	0.20	0.10	0.88825	0.40958
1.0	2.0	0.1	3.5	0.20	0.10	0.20	0.10	0.82258	0.43953
1.0	2.0	0.1	2.0	0.05	0.10	0.20	0.10	0.96929	0.06229
1.0	2.0	0.1	2.0	0.10	0.10	0.20	0.10	0.89431	0.24939
1.0	2.0	0.1	2.0	0.15	0.10	0.20	0.10	0.74687	0.50994
1.0	2.0	0.1	2.0	0.20	0.11	0.20	0.10	0.78130	1.02362
1.0	2.0	0.1	2.0	0.20	0.12	0.20	0.10	1.03618	1.24281
1.0	2.0	0.1	2.0	0.20	0.13	0.20	0.10	1.31938	1.48079
1.0	2.0	0.1	2.0	0.20	0.10	0.17	0.10	1.27100	−0.00377
1.0	2.0	0.1	2.0	0.20	0.10	0.18	0.10	1.00897	0.29162
1.0	2.0	0.1	2.0	0.20	0.10	0.19	0.10	0.76983	0.56557
1.0	2.0	0.1	2.0	0.20	0.10	0.20	0.12	0.36255	0.76575
1.0	2.0	0.1	2.0	0.20	0.10	0.20	0.13	0.25859	0.72530
1.0	2.0	0.1	2.0	0.20	0.10	0.20	0.14	0.14691	0.67433

5 Conclusion

This study aims to determine the influence of a heat source/sink on a non-Newtonian hybrid nanofluid saturated with a porous medium separated between the transparent viscous fluid filled in a vertical channel. The main goal of this research is to depict the blood-based nanofluid flow properties after the mechanism has been filled with nanoparticles. The influence of distinctive factors like the Casson parameter, Grashof number, frequency parameter, porous parameter, Eckert number, nanoparticle volume fraction, heat source/sink parameters, and time parameter are shown through two-dimensional graphs and tables. The following significant findings emerged from this investigation:

- Improving Casson parameter β tends to increase the steady $U_s(\zeta)$ and unsteady velocity profiles $U_t(\zeta)$.
- Velocity profiles decrease with increasing amounts of Grashof number, and the opposite nature is observed for the temperature profiles.
- The velocity profile $U_s(\zeta)$ is diminished by expanding values in the porosity parameter σ.
- The higher values of t diminish all three regions of the $U_t(\zeta)$, and the contrary nature is detected for $\theta_t(\zeta)$.